

Self-sustained irregular activity in an ensemble of neural oscillators

Ekkehard Ullner^{1,*} and Antonio Politi^{1,†}

¹*Institute for Complex Systems and Mathematical Biology and SUPA,
University of Aberdeen, Aberdeen AB24 3UE, United Kingdom*

(Dated: August 23, 2021)

An ensemble of pulse-coupled phase-oscillators is thoroughly analysed in the presence of a mean-field coupling and a dispersion of their natural frequencies. In spite of the analogies with the Kuramoto setup, a much richer scenario is observed. The “synchronized” phase, which emerges upon increasing the coupling strength, is characterized by highly-irregular fluctuations: a time-series analysis reveals that the dynamics of the order parameter is indeed high-dimensional. The complex dynamics appears to be the result of the non-perturbative action of a suitably shaped phase-response curve. Such mechanism differs from the often invoked balance between excitation and inhibition and might provide an alternative basis to account for the self-sustained brain activity in the resting state. The potential interest of this dynamical regime is further strengthened by its (microscopic) linear stability, which makes it quite suited for computational tasks. The overall study has been performed by combining analytical and numerical studies, starting from the linear stability analysis of the asynchronous regime, to include the Fourier analysis of the Kuramoto order parameter, the computation of various types of Lyapunov exponents, and a microscopic study of the inter-spike intervals.

PACS numbers: 05.45.-a, 87.19.lj, 05.45.Xt

I. INTRODUCTION

Most of the challenging questions that arise in the attempt of improving our understanding of the natural (and artificial) world deal with multi-component systems, whose overall dynamics is the result of many nonlinear interactions. The difficulty of the task is often mitigated by the assumption of being before universal phenomena, which do not crucially depend on the details of the underlying models. It is therefore customary to deal with relatively simple setups in the hope that relevant details are not missed.

The mammalian brain is the most prominent example where this approach is absolutely necessary, if we wish to make some substantial progress. There, even after disregarding several ingredients, such as the multiple degrees of freedom involved in the dynamics of realistic neurons (as in multicompartmental models [1]), the diversity among the single units, the topology and the plasticity of the connections, the range of possible dynamical phenomena is still very rich and not yet entirely understood. Self-consistent partial synchronization is a simple but enlightening example. The phenomenon, discovered by van Vreeswijk in an ensemble of leaky integrate-and-fire neurons (LIF) [2], was believed for a long time to be a non-perturbative effect. Only, recently it has been however clarified [3] that it is equivalent to the rotating waves observed in the weak-coupling limit [4], and can indeed be observed and characterized in Kuramoto-Daido oscillators [5], as well.

In general, the problem of characterizing the collective dynamics of an ensemble of oscillators is deeply connected to the question of how different levels of descriptions are linked to one another. In computational neuroscience, it is customary

to consider subpopulations of neurons, under the assumption that the firing rate is the single relevant variable, as in the seminal paper by Wilson and Cowan [6] and in several other publications (see e.g. [1, 7, 8]). It is not, however, clear whether such models can be derived starting from more microscopic setups based on single spiking neurons. Some recent studies have shown that a low-dimensional collective dynamics may emerge in networks of theta (or, equivalently, quadratic-integrate-and-fire, QIF) neurons [9, 10]. More than that, a reformulation of pulse-coupled oscillators in terms of firing-rate models has been accomplished in [11, 12]. The validity of these results is due to the existence of relationships such as the Ott-Antonsen Ansatz [13] and the Watanabe-Strogatz theorem [14], which allow expressing the collective behavior in terms of a few variables, the others being essentially slaved. Such theoretical pillars are however based on strong simplifying assumptions on the nature of the inter-oscillator coupling [13, 14].

To what extent is the compression of degrees of freedom effective in more general setups? The background activity of the brain in the resting state, when no specific task is performed [15–17] testifies to a collective irregular dynamics. Moreover, the ongoing discussion about rate- versus temporal-coding [18, 19], suggests that the firing rate may not be sufficient to ensure the necessary computational capability of the mammalian brain.

Altogether, one should thus expect an irregular collective behavior. It is often conjectured that the self-sustained activity is the result of a balance between activation and inhibition [20, 21]. Mathematically, this means that the effect of the coupling is zero on average so that it is essentially controlled by stochastic/chaotic fluctuations. It is not, however, clear how such a balance can be durably ensured in self-organized networks of firing oscillators. A conceptually different possibility to account for a macroscopic irregularity is offered by the nonlinear character of the Liouville-type equation (which, strictly speaking, applies to an ensemble of infinitely many

* e.ullner@abdn.ac.uk

† a.politi@abdn.ac.uk

oscillators). This functional equation operates in an infinite-dimensional phase space and can, thereby, generate a dynamics of arbitrary complexity. This has been indeed observed in an abstract model of coupled maps [22] and in globally coupled Stuart-Landau oscillators [23]. In both cases, the single dynamical units are intrinsically more complex than phase oscillators: the logistic maps are chaotic by themselves, Stuart-Landau oscillators can behave chaotically under the action of a periodic modulation. In the case of phase oscillators, there is only a preliminary evidence in an ensemble of LIF neurons with delayed interactions [24].

In this paper, we present a model whose overall activity is intrinsically highly-dimensional. As this dynamical phase is rather robust against variations of several parameters, it may provide an alternative mechanism for the self-sustainment of the resting brain activity. More precisely, we study an ensemble of pulse-coupled phase oscillators, whose phase-response curve (PRC) is derived by smoothing the PRC of LIF neurons. Other than that, our setup is the same as in the standard Kuramoto model [25, 26]: the single oscillators are characterized by a distribution of bare frequencies, while the coupling is homogeneously all-to-all. As in the Kuramoto model, a synchronization transition is observed upon increasing the coupling strength, but the analogies end here, since above criticality, the order parameter, rather than being constant, exhibits complex high-dimensional oscillations. Such fluctuations are present in the “activity” field as well, a variable akin to the electric potential recorded while measuring EEGs.

As briefly discussed in section III, in the weak-coupling limit (and for a small dispersion of the frequencies), our system reduces to a Kuramoto-Daido model, with the coupling function being composed of several Fourier harmonics. Recent studies of such a type of models have revealed quite a rich phenomenology (see, e.g. [27, 28]). This is not, however, sufficient to account for the qualitative differences reported in this paper: direct simulations show that the scenario hereafter discussed disappears when the dispersion of frequencies is decreased.

More specifically, the overall dynamics is characterized by a spectrum of negative Lyapunov exponents. This *inconsistency* is nothing but a manifestation of stable chaos [29], an irregular dynamics of cellular-automaton type, which is self-sustained because of the high (infinite) dimensionality of the phase space (in other words, it dies out in finite ensembles). In neural systems, stable chaos was first found in a diluted network of LIF units [30], and later discussed in more disordered setups [31, 32]. At variance with deterministic chaos, accompanied by an exponential separation of orbits and thereby a loss of memory, stable chaos is identified by a “microscopically” stable dynamics, which is definitely more appropriate for the performance of computational tasks. The potentiality of stable chaos for information processing has been preliminarily explored in [33, 34]. The onset of a macroscopic irregular dynamics, as discussed in this paper, makes this perspective even more intriguing, for the richness of the collective behavior.

In section II we introduce the setup and justify its choice. In the following section III we reconstruct the asynchronous

state and investigate its stability properties. Differences and analogies with the standard Kuramoto model are emphasized. In particular, we find that the asynchronous regime loses its stability when a complex eigenvalue is born out of the line containing the continuous spectrum. In the last part of the section, the proper order parameters for the characterization of the transition are introduced: they are the Kuramoto order parameter, whose definition requires passing to more appropriate phase variables, and the activity field. Sections IV and V are devoted to a careful numerical analysis of the synchronized phase at the collective and microscopic level, respectively. Due to the difficulty of dealing with finite-size corrections, we study the resulting behavior sufficiently far from the transition. In section IV we first illustrate the phase diagram and the initial part of the Lyapunov spectrum. We then show the power spectrum of the order parameter and carry on a time-series analysis to determine the fractal dimension. In section V we focus our interest on the behavior of the single neurons, computing the effective frequency and the conditional Lyapunov exponents: they are all negative, indicating that we are in the presence of generalized synchronization. The presence of phase slips is also unveiled. Finally in the last section we summarize the main results and discuss the several perspectives that are opened by the scenario discussed in the paper.

II. THE MODEL

The starting point of this paper is the model of delayed LIF neurons studied in [24]. Here, the model is modified to make it simpler, more generic and more amenable to both numerical and analytical studies.

In this perspective, we consider an ensemble of pulse-coupled phase oscillators, in the presence of δ -like pulse and characterized by a suitable PRC $\Gamma(\phi)$,

$$\dot{\phi}_i = \omega_i - \frac{g}{N} \Gamma(\phi_i) \sum_j \delta(t - t_j), \quad (1)$$

where $\phi_i \in [0, 1]$ is the local phase, ω_i the bare oscillator frequency (i.e. in the absence of coupling), g the coupling strength and N is the system size. Whenever any oscillator reaches the threshold $\phi_i = 1$, a δ -spike is sent and received by all neurons. The above formulation is quite general for two reasons: (i) any model where the velocity field $\dot{\phi}_i$ is phase dependent (in the absence of coupling), can be always rephrased as Eq. (1) upon suitably changing variables [35]; (ii) finite-width pulses can be mapped onto δ -like ones, upon suitably adjusting the shape of the PRC [3] (at least in the weak coupling limit).

An important ingredient of the model studied in [24] is the presence of a delay between spike emission and reception. In the weak-coupling limit, when the dynamics is nearly homogeneous, one can simulate the presence of a delay as a suitable phase shift of the PRC and this is what has been assumed here. The phase shift should be different for the different oscillators. However, here, for the sake of simplicity we assume the same PRC for all the oscillators.

In the LIF model, $\Gamma(\phi_i) = a \exp(b\phi_i)$ where ϕ_i is assumed to be taken modulus 1. As a result of a phase shift, the discontinuity originally present when passing from 1 to 0, moves inside the unit interval. For the sake of generality and simplicity, we prefer to remove the discontinuity, considering a piece-wise linear PRC, such as

$$\Gamma(\phi) = \begin{cases} B_{01} + b_1\phi & \text{if } 0 \leq \phi < \phi_l \\ B_{02} - b_2\phi & \text{if } \phi_l \leq \phi \leq \phi_r \\ B_{03} + b_1\phi & \text{if } \phi_r < \phi < 1, \end{cases} \quad (2)$$

where the various parameters are chosen so as to ensure continuity in ϕ_l , ϕ_r and equality between $\phi = 0$ and 1. Considering that the amplitude of the PRC is controlled by the coupling constant g , there are three truly independent parameters: one controlling the vertical shift of the PRC, and two which identify the junction points. As for the first parameter, it basically controls whether the coupling has an average excitatory or inhibitory effect, thereby inducing a speeding up or slowing down of the spiking activity. Since we are not interested in such effects, but rather in the mutual attraction or repulsion among the oscillators, we have decided to assume that the PRC has zero average. The two remaining parameters are identified by the phase shift s (defined as the distance of the midpoint of the central region from 1 - see the Fig. 1) and the width δ of the central interval. Altogether, $b_2 = b_1/\delta$, $B_{01} = b_1(s - 1/2)$, $B_{02} = b_1(1 - s)/\delta$, $B_{03} = b_1(s - 3/2)$, while $\phi_l = (1 - s + \delta/2 - \delta s)/(\delta + 1)$ and $\phi_r = (1 - s + 3\delta/2 - \delta s)/(\delta + 1)$. The parameter b_1 has been set equal to 1.5 (in principle, it can be absorbed in the definition of g), while the two other parameters have been set $s = 0.14$, $\delta = 0.1$ in all of the following simulations. The resulting shape of the PRC is presented in Fig. 1.

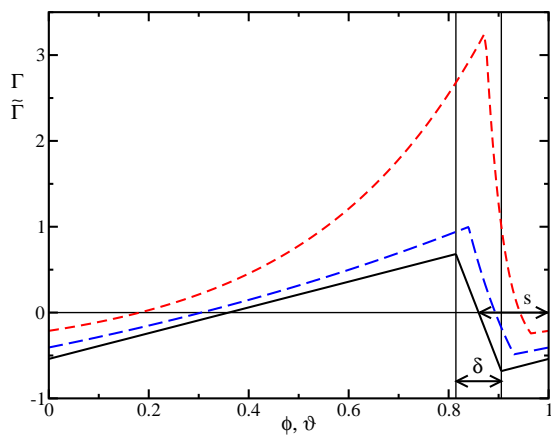


FIG. 1. Phase response curve $\Gamma(\phi_i)$ according to Eq. (2) for the standard parameter values $b_1 = 1.5$, $s = 0.14$, and $\delta = 0.1$ (solid line); the short- and long-dashed curves correspond to the effective PRC $\tilde{\Gamma}$ obtained for $\omega = \omega_{min} = 0.8$ and $\omega = \omega_{max} = 2$, respectively (with $g = 0.8$).

Finally, we have chosen to work with a uniform distribution of frequencies centered in $\bar{\omega} = 1.4$. The simulations reported

in this paper refer to a half width $\Delta = (\omega_{max} - \omega_{min})/2 = 0.6$, but similar results have been obtained for different values of Δ . We evolve the model Eq. (1,2) as an event driven process. Between two consecutive δ -spikes, the phase of each oscillator increases linearly according to its individual bare frequency ω_i . When one of the oscillators reaches the firing threshold $\phi_i = 1$, its phase is reset to zero and all phases are adjusted to account for the received spike. The effect of the coupling might bring a second oscillator beyond the firing threshold. In such a case, also that oscillator is reset to zero plus an offset due to the spike received from the first oscillator. We continue this evolution, without advancing the time, until no further spikes are triggered. In practice, “avalanches” may occur: we have controlled that they do not contribute significantly to the global behavior as their size does not increase upon increasing the number of neurons. Notice also that in the original model [24], avalanches do not exist.

III. THEORY

Some insight can be gained by considering the thermodynamic limit, as this allows determining analytically the properties of the stationary asynchronous regime.

First of all it is convenient to define the activity field $E(t)$ as the number of spikes emitted per unit time, so that Eq. (1) can be rewritten as (for the sake of simplicity we drop the subindex i),

$$\dot{\phi} = \omega - g\Gamma(\phi)E(t). \quad (3)$$

Let us now introduce the probability density $Q(\phi, \omega, t)$, as the fraction of neurons with a bare frequency in $[\omega, \omega + d\omega]$, whose phase belongs to $[\phi, \phi + d\phi]$ at time t . Clearly,

$$\int Q(\phi, \omega, t) d\phi = P(\omega),$$

where $P(\omega)$ is the density of neurons with bare frequency ω . Q satisfies the continuity equation

$$\frac{\partial Q}{\partial t} = -\frac{\partial}{\partial \phi} [\omega - g\Gamma(\phi)E(t)] Q, \quad (4)$$

while the field E satisfies the self-consistent equation

$$E(t) = \int Q(1, \omega, t) [\omega - g\Gamma(1)E(t)] d\omega, \quad (5)$$

which implies

$$E(t) = \frac{\int \omega Q(1, \omega, t) d\omega}{1 + g\Gamma(1) \int Q(1, \omega, t) d\omega}.$$

The asynchronous regime corresponds to the stationary solution whose phase-dependence is determined by setting the time derivative of Q equal to zero. By properly renormalizing the flux, one obtains

$$Q_0(\phi, \omega) = \frac{P(\omega)}{T(1, \omega) [\omega - g\Gamma(\phi)E_0]}, \quad (6)$$

where

$$T(\psi, \omega, E_0) = \int_0^\psi \frac{d\phi}{\omega - g\Gamma(\phi)E_0} \equiv \int_0^\psi d\phi \tau(\phi, \omega) \quad (7)$$

is the time required by an oscillator with frequency ω to reach the phase ψ , starting from 0, in the presence of a constant field E_0 . $T(1, \omega, E_0)$ is thereby the interspike interval, while $\tau(\phi_i, \omega)$ is the inverse instantaneous effective frequency. The field E_0 can be finally obtained from Eqs. (5,6)

$$E_0 = \int \frac{P(\omega)}{T(1, \omega)} d\omega. \quad (8)$$

The above calculation yields the structure of the asynchronous state, but it does not tell us whether it is stable. The stability can be assessed by investigating the behavior of infinitesimal perturbations. Let us define,

$$Q(\phi, \omega, t) = Q_0(\phi, \omega) + q(\phi, \omega, t) \quad , \quad E(t) = E_0 + e(t)$$

q and e satisfy the following equations,

$$\frac{\partial q}{\partial t} = -\frac{\partial}{\partial \phi} [\omega - g\Gamma(\phi)E_0] q + ge(t) \frac{\partial \Gamma(\phi)Q_0}{\partial \phi}$$

and

$$e(t) = \frac{\int (\omega - g\Gamma(1)E_0)q(1, \omega, t)d\omega}{1 + g\Gamma(1) \int Q_0(1, \omega)d\omega}.$$

These two equations can be solved by introducing a standard Ansatz, $q(\phi, \omega, t) = u(\phi, \omega)e^{\mu t}$, $e(t) = ze^{\mu t}$. One obtains

$$\mu u = g\Gamma' E_0 u - [\omega - g\Gamma E_0] u' + g\Gamma' Q_0 z + g\Gamma Q_0' z \quad (9)$$

and

$$z = \frac{\int (\omega - g\Gamma(1)E_0)u(1, \omega)d\omega}{1 + g\Gamma(1) \int Q_0(1, \omega)d\omega}, \quad (10)$$

where the prime denotes a derivative with respect to ϕ and we have dropped the dependence on ϕ for the sake of simplicity. The solution of such equation, reported in the appendix A, yields the eigenvalue equation (A9).

The spectrum of the linear operator consists of a continuous and a discrete component. The continuous part is confined to an interval along the imaginary axis and is therefore composed of marginally stable directions. The discrete component can be obtained by assuming $\mu = \mu_R + i\mu_I$, separating (A9) into real and imaginary parts, and finally looking for the zeros in the complex plane.

A numerical study reveals the presence of (at least) three pairs of complex-conjugate eigenvalues (see Fig. 2, where the imaginary part is not reported) two of which being negative and one positive. Two pairs of exponents arise definitely above some finite g value; the third one is likely to follow the same scenario, but given its small real part we could not trace it for small coupling strengths (see the crosses in Fig. 2). Altogether, the asynchronous solution is marginally stable up until $g_c \approx 0.72$, when it destabilizes for the onset of a pair of complex conjugate eigenvalues with a positive real part.

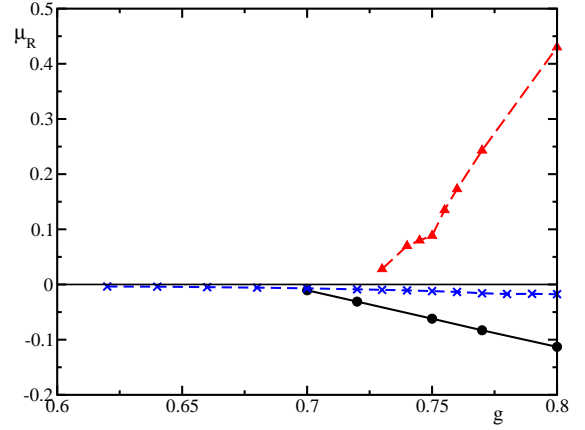


FIG. 2. Stability diagram of the asynchronous state. The real part of the discrete eigenvalues is reported versus the coupling strength g .

Let us now compare with the stability of the asynchronous solution in the Kuramoto model. Below criticality, in both cases the probability distribution is marginally stable (see [36] for the first such analysis in the Kuramoto setup), the major difference being the presence of a discrete stable spectral component in our model. Noteworthy, in spite of the marginal stability of the probability density, the order parameter (see the next section for its definition) relaxes exponentially in the Kuramoto model. This is a manifestation of the so-called Landau damping [37]. Only recently this “inconsistency” has been fully resolved, by understanding that different classes of functions may be considered in the stability analysis [38–40]. We do not know how much of such studies carry over to the present setup: this is an open problem.

At criticality, a pair of complex eigenvalues with a positive real part is born: this is at variance with the standard Kuramoto model, where the newly appearing eigenvalue is real. There is, instead, an analogy with the Kuramoto model with delay [41, 42], where periodic oscillations arise. Here, however, above threshold, the probability density rather than oscillating periodically, behaves irregularly, as discussed in the following sections.

A. Order parameters

In order to study the transition, it is necessary to identify a suitable order parameter. One cannot directly use the phase ϕ to define the Kuramoto order parameter [25], since in the asynchronous regime, such phases do not advance homogeneously in time, i.e. they are not proper phases. This can be accomplished by introducing the new variable ϑ

$$\frac{d\vartheta}{d\phi} = \frac{\tau(\phi, \omega)}{T(1, \omega, E_0)} \quad (11)$$

that is basically equivalent to the elapsed time (apart from a scaling factor) and thus advances uniformly by definition.

With reference to this new phase, the local dynamics is described by the equation

$$\dot{\vartheta} = \tilde{\omega} - g\tilde{\Gamma}(\vartheta)(E(t) - E_0), \quad (12)$$

where $\tilde{\Gamma}(\vartheta)$ is the effective PRC

$$\tilde{\Gamma}(\vartheta) = \frac{\tilde{\omega}\Gamma(\phi(\vartheta))}{\omega - gE_0\Gamma(\phi(\vartheta))}, \quad (13)$$

$\vartheta(\phi)$ is obtained by solving Eq. (11), and $\tilde{\omega} = 1/T(1, \omega, E_0)$, is the effective frequency. As it is understood from its definition $\vartheta(\phi)$, depends both on g and the bare frequency. The dependence of ϑ on ϕ is reported in Fig. 3 for the maximal and minimal frequencies at $g = 0.8$. The particular transformation from the phase ϕ to the new effective phase ϑ is shown in the appendix B.

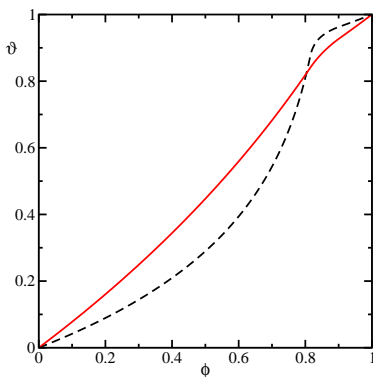


FIG. 3. $\vartheta(\phi)$ for $g = 0.8$ and two different frequencies: $\omega = 0.8$ (dashed curve) and $\omega = 2$ (solid curve).

Once a proper phase ϑ has been identified, a meaningful Kuramoto order parameter can be defined,

$$R = \frac{1}{N} \sum_j e^{2\pi i \vartheta_j}.$$

Since $R = 0$ in the asynchronous regime, it can be safely used to identify the onset of even weak forms of synchronization.

Given the large amount of transformations needed to determine R , and because of the relationship with neural networks, we have often considered a second order parameter, a smoothed version $Y(t)$ of the field $E(t)$. In a finite system, $E(t)$ is just a collection of δ -pulses. It is therefore more convenient to investigate

$$\dot{Y} = -\gamma Y + E(t).$$

We have selected $\gamma = 5$. In the asynchronous regime, the activity is constant, i.e. $Y_0 = E_0/\gamma$. Above the transition that we are going to discuss, the activity starts oscillating in time, so that it is convenient to introduce the temporal standard deviation

$$\sigma_Y = \sqrt{\langle Y^2 \rangle - \langle Y \rangle^2},$$

where the angular brackets denote a time average. It will be also useful to look at the fluctuation σ_R of the Kuramoto order parameter R , as this indicator allows identifying the regimes where the degree of synchronization oscillates in time.

We end this theoretical section by briefly commenting on the weak-coupling, low-disorder limit. The effective PRC $\tilde{\Gamma}$ depends on the frequency of the oscillator (and on the coupling strength). The resulting curves for ω_{min} and ω_{max} (and $g = 0.8$) are reported in Fig. 1: see the dashed lines. In the small-disorder limit, one can neglect such a dependence. By then following, Ref. [3], we expect the model to become equivalent to the Kuramoto-Daido model

$$\vartheta_i = \omega_i - \frac{g}{N} \sum_j \tilde{\Gamma}(\vartheta_i - \vartheta_j).$$

The above equation makes one difference with the Kuramoto model transparent: the sinusoidal coupling function is replaced by the more structured function $\tilde{\Gamma}$ (see Fig. 1). This is not, however, the major source of differences, since the simulations show that the weak-disorder assumption is not appropriate to reproduce the scenario discussed in this paper.

IV. MACROSCOPIC DYNAMICS

The most appropriate control parameter to study the onset of collective dynamics is the coupling strength g . In Fig. 4a,b, it is used to parametrize the dependence of the Kuramoto order parameter R , its temporal standard deviation σ_R , and the standard deviation of the activity field Y .

Each data point is based on a simulation over 500 time units after a transient of 50 time units. All, but the red curve, have been obtained by increasing the coupling strength g stepwise, using the final condition for a given g value as the initial condition for the next one. The statistical uncertainty (represented by the error bars) has been estimated by dividing the standard deviation of the Kuramoto order parameter by the square root of the number N_e of effectively independent time intervals and N_e has been in turn determined as the ratio between the total length of the time series by the decay time of the auto-correlation function. A long correlation time for $g = 1$ (≈ 250 units) causes the large error compared to smaller ($g = 0.8$) and larger coupling ($g = 1.3$).

The simulations performed for three different system sizes (4000, 16000 and 64000 units) reveal the existence of a critical g -value above which R grows from zero, as in the usual Kuramoto setup and that this value is in good agreement with g_c as estimated from the linear stability analysis discussed in the previous section. At variance with the Kuramoto model, here, the standard deviation σ_R is larger than zero, meaning that the degree of synchronization oscillates in time already slightly above threshold. Finally, σ_Y exhibits the same behavior as σ_R , confirming that the transition is accompanied by the onset of macroscopic oscillations.

Finally, the red curve tracks the mean-field obtained by decreasing g . The difference observed in the critical region with respect to the previous curves (obtained by increasing g) sug-

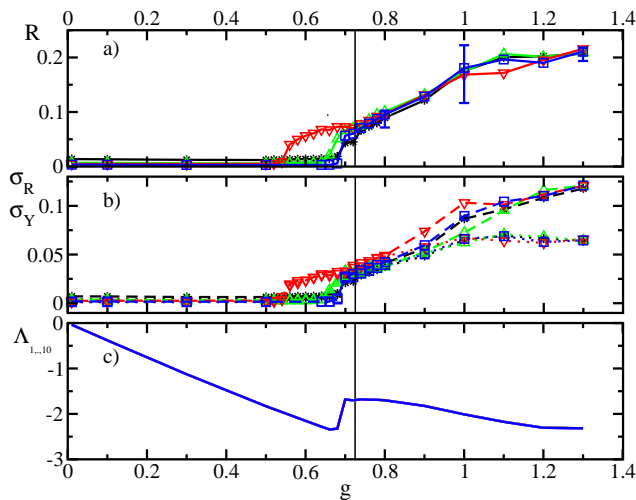


FIG. 4. Phase diagram: Dependence of the Kuramoto order parameter R (a), its standard deviation σ_R , the standard deviation σ_Y of the activity field Y (b), and the ten largest Lyapunov exponents versus the coupling strength g . The curves in a and b have been obtained for $N = 4000$ (black), $N = 16000$ (green) and $N = 64000$ (blue), upon increasing the coupling g . The red curve (a and b) is a continuation by decreasing g with $N = 64000$. σ_R and σ_Y are represented with dashed and dotted lines, respectively (b). The vertical lines mark the critical point $g_c \approx 0.72$, where the linear stability of the asynchronous state is lost (see section III). The ten largest global Lyapunov exponents in panel c are almost indistinguishable. The simulations have been performed for $N = 64000$, increasing g .

gests the possible co-existence of an asynchronous with a partially synchronised regime. Since, however, no jump is observed in the simulations performed by increasing g , it is reasonable to conclude that the bifurcation is “supercritical” and thus to attribute such deviations to the finite sweeping time. Anyway, since the main goal of this work is to characterise the behavior above threshold, we have preferred to focus our efforts on larger g -values, where the asymptotic regime is much less dependent on the selection of the initial condition.

A first qualitative instance of the collective dynamics can be appreciated in Fig. 5, where $R(t)$ and $Y(t)$ are plotted for $g = 1.3$ showing that the evolution is more complex than just periodic.

A more quantitative characterization of the collective temporal behavior can be obtained by looking at power spectra. The square amplitude of the Fourier transform of $Y(t)$ is reported in Fig. 6 for two different coupling strengths.

There we see that the spectra possess quite a rich structure, being neither trivially broad-band, nor just revealing a periodic behavior (especially for $g = 0.8$). A closer look at the width of the various peaks upon increasing the network size reveals that they do not decrease. Simulations performed for different realization of the bare frequencies (data not shown) indicate that the results are almost independent, especially for the larger system sizes. Altogether, we are thus led to conclude that the stochastic-like dynamics is not due to finite-size effects, but intrinsic of the thermodynamic limit.

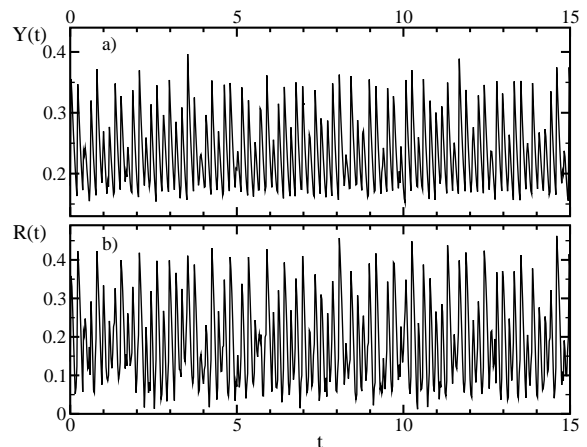


FIG. 5. Time evaluation of Y (a) and R (b) for $g = 1.3$ and system sizes: $N = 4000$.

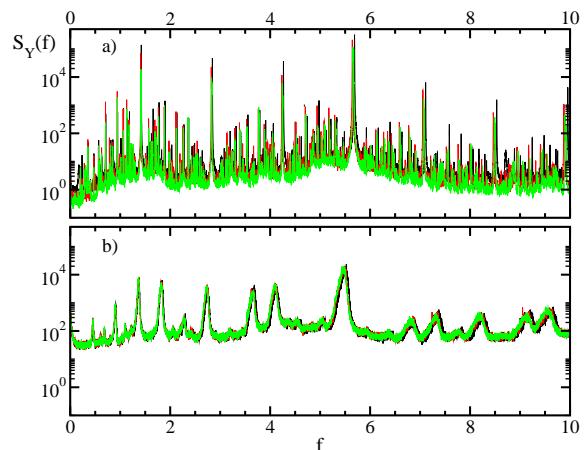


FIG. 6. Power spectra of Y for $g = 0.8$ (a), and 1.3 (b) in each case for: $N = 4000$ (black), $N = 16000$ (red) and $N = 64000$ (green). The spectra are obtained by transforming time series of 819.175 time units, sampled every 0.025 units and averaged over 50 different realizations.

According to the theory of nonlinear dynamical systems, it is well known that an irregular evolution may well be the manifestation of low-dimensional deterministic chaos. Can it be the case here? In order to clarify the point, it is natural to investigate the behavior of the activity field by performing a nonlinear time series analysis, to determine its fractal dimension. Given a time series $Y(t_n)$, sampled at equally spaced times ($\Delta t = t_{n+1} - t_n = 0.025$), one starts embedding the series into a space of dimension m , by building vectors of the type $[Y(t_n), Y(t_{n+s}), \dots, Y(t_{n+(m-1)s})]$, where s is suitably selected. As often done, we have chosen s , so that $s\Delta t$ is close to the first minimum of the autocorrelation of $Y(t)$ ($s = 5$, in our case).

The fractal dimension has then been estimated by using the nearest-neighbour method [43], as it suffers of less fluctua-

tions in the region of small distances. Given a generic time series, N_r reference points are randomly selected ($N_r = 10^5$ in our case). Each of them is compared with an increasing number n of randomly selected measurement points (the other points in the time series - up to a maximum $N_m = 16 \cdot 10^6$), monitoring the distance $\varepsilon_m(k, n)$ of the k -th neighbour (the distance is herein estimated using the maximum norm), for different values of the embedding dimension m and k . A well established theory [43], implies that for large n

$$\langle \ln \varepsilon_m(k, n) \rangle \approx \frac{\ln n}{D_e},$$

where the angular brackets denote the average over the reference points, while D_e is the (effective) information dimension. In order to make the dependence of D_e on the resolution ε_m transparent, we have modified the standard approach. Once interpreted the logarithmic derivative of n as a resolution-dependent dimension,

$$D_e(\varepsilon_m) = \frac{d \ln n}{d \langle \ln \varepsilon_m \rangle},$$

we have plotted it versus $\langle \varepsilon_m \rangle$ itself, interpreted as an independent variable. In fact, we have verified that $D_e(\varepsilon_m)$ takes the same value, irrespective of the way ε_m has been determined (i.e. independently of the k value). The only differences are that larger k -values yield smaller statistical fluctuations, but are confined to larger distances. A good compromise has been obtained by gluing together the data obtained for the largest k value (30) with the data obtained for the smallest distances and a lower-order neighbour (4th one).

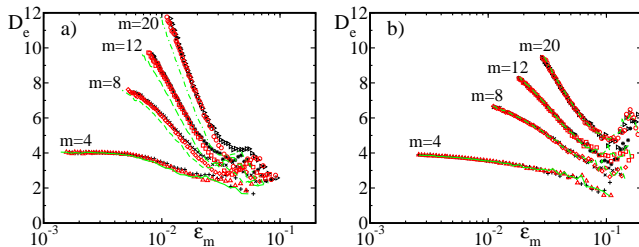


FIG. 7. Effective dimension D_e as a function of the resolution ε_m for $g = 0.8$ and $g = 1.3$ in panel a and b, respectively. The system size is $N = 4000$ (black), $N = 16000$ (red) and $N = 64000$ (green). The different symbols belong to different embedding dimensions m marked in the figure. The curves for the same embedding dimension group together with a similar slope irrespective of the system size.

The results for $g = 0.8$ are reported in Fig. 7a and different ensemble sizes ($N = 4000, 16000$, and 64000). The first point to notice is that for the lowest embedding dimension ($m = 4$), D_e nicely converges to 4 upon decreasing ε . This clearly implies that the dimension of the collective motion is at least 4, i.e. one needs at least four variables to characterize such a behavior. Furthermore, the curves obtained for the larger m values, reveal an increase, each possibly hinting to m , thus suggesting that the dynamics is high-dimensional (if

not even infinite dimensional). Additionally, one can also appreciate a small shift to smaller scales of the curves obtained for $N = 64000$. In itself, this is the indication of finite-size effects. If the shift continues as such by further increasing m , it would mean that part of the high-dimensionality is just a consequence of statistical fluctuations which disappear in the thermodynamic limit. We are more inclined to attribute such discrepancies to another type of finite-size effect: a non perfect equivalence among the various realizations of the frequency distributions. We have, in fact, observed that different clusters may temporarily form during the evolution, especially in the interval $g \in [g_c, 1.2]$ (see a more detailed discussion in section V).

For $g = 1.3$ the convergence to the thermodynamic limit is more clear. In Fig. 7b the agreement among the different network sizes is compelling over a wide range, suggesting thus that the statistical fluctuations do not affect the dimension estimates. We have, also, double-checked the results by computing the correlation dimension with the TISEAN package [44]: a rather similar pattern emerges (data not shown).

Finally, we have investigated the degree of (in)stability of the dynamics, computing the first 10 Lyapunov exponents Λ_j . We have followed the approach described in [45], which consists in formally interpreting the time evolution as a series of discrete-time maps from one to the next spike emission. The results are plotted in Fig. 4c upon varying the coupling strength. There we see that the dynamics is always stable (notice that the zero Lyapunov exponent, always present in a non-constant autonomous dynamics is automatically discarded). For a vanishing g , all the Lyapunov exponents converge to zero: this is obvious, since in this limit all the oscillators are uncoupled. Much less trivial is that the Lyapunov exponents are all negatives in spite of a dynamics that may even be collectively irregular. This manifestation of stable chaos strongly suggests that the connection between different levels of descriptions (micro vs. macroscopic) of a given model is weak, if any.

V. MICROSCOPIC DYNAMICS

In this section we try to shed light on the collective dynamics by analysing the behavior of the single neurons. We start noticing that the coupling modifies the firing rate of the neurons. This can be appreciated in Fig. 8a, where the effective (average) frequency $\tilde{\omega}$ is reported for the coupling strength $g = 1$. The dashed line corresponds to the bare frequency of each neuron. Almost everywhere $\tilde{\omega}$ is smaller than the bare frequency ω . This is a consequence of the fact that, although the PRC was chosen to be symmetric around zero, this is no longer true for the effective PRC (see Fig. 1). The most interesting feature to notice is, however, the staircase structure of $\tilde{\omega}(\omega)$ with flat plateaus which correspond to clusters of mutually synchronised neurons: the synchronization does not mean a perfect phase locking but that the phase differences never become larger than 2π .

One way to characterize the irregularity of the single-neuron activity is through its coefficient of variation (CV), i.e.

the standard deviation of the the inter-spike interval rescaled to its average value. In Fig. 8b, we see that the CV allows identifying synchronized clusters as those frequency intervals where the fluctuations are significantly smaller. Furthermore, distinct lines can be recognized inside some clusters: they correspond to different locked states [46] and are a manifestation of the multistability that is in fact seen also at the macroscopic level. On a more quantitative level, the neural dynamics is not significantly irregular if compared, for instance, to the true brain activity in the resting state. It should be, however, kept in mind that in our toy model, the only source of disorder is the distribution of bare frequencies; no disorder has been assumed in the synaptic connections.

Additional information can be extracted by assuming that the self-determined activity field $E(t)$ is externally given, so that each neuron can be interpreted as a forced dynamical system. In this way, it is natural to compute the (conditional) Lyapunov exponent λ_i . In Fig. 1c, one can observe a scenario that is qualitatively different from what observed in the Kuramoto model: all λ_i 's are negative, including those of the neurons outside the flat plateaus. We come back to this point ahead in this section.

A partially different scenario is found for $g = 1.3$ (see Fig. 8d-f). First of all any sign of multistability has disappeared and all plateaus as well. The initial high peak of the CV (panel e) is due to the fact that now the neurons with the lowest bare frequency do not spike at all, having undergone a kind of oscillation-death. Their CV is obviously equal to zero. As a result, the first erratically spiking neurons are characterized by long interspike intervals and are obviously accompanied by large fluctuations. The CV of these rarely firing neurons is as large as 1.75 (not shown in Fig. 8e with the present scale). The kind of oscillation-death phenomena could be seen as an inhomogeneous limit cycle (IHLC) because non spiking neurons are not trapped at a steady state, rather moving back and forth according to their bare frequency and the global pulses, never reaching the threshold [47]. Hence we observe two groups of neurons, the quiet neurons but still being sub-thresholdly active and the firing neurons. The situation is a more complicated than usual IHLC, because of the many (in the thermodynamic limit infinite many) frequencies reflected in the power spectra (Fig. 6). Moreover, the dynamics of each oscillator is rather stable.

Altogether, the microscopic analysis confirms that the microscopic behavior is linearly stable: each neuron is synchronized with the self-generated mean-field $E(t)$ and yet an irregular dynamics is self-sustained. This can be understood by noticing that in many frequency ranges, the effective frequency is a strictly monotonous function of ω . This means that, even though each neuron synchronizes with the field E , the parameter (bare frequency) mismatch induces a qualitatively different response: such qualitative differences are then responsible for the maintenance of the self-generated irregularity. In a more technical way: the response of a phase oscillator is not structurally stable: one can slightly modify its frequency and still observe significant changes (phase-slips). A more physical (although still qualitative) way to understand the phenomenon is as follows: one can see each phase-

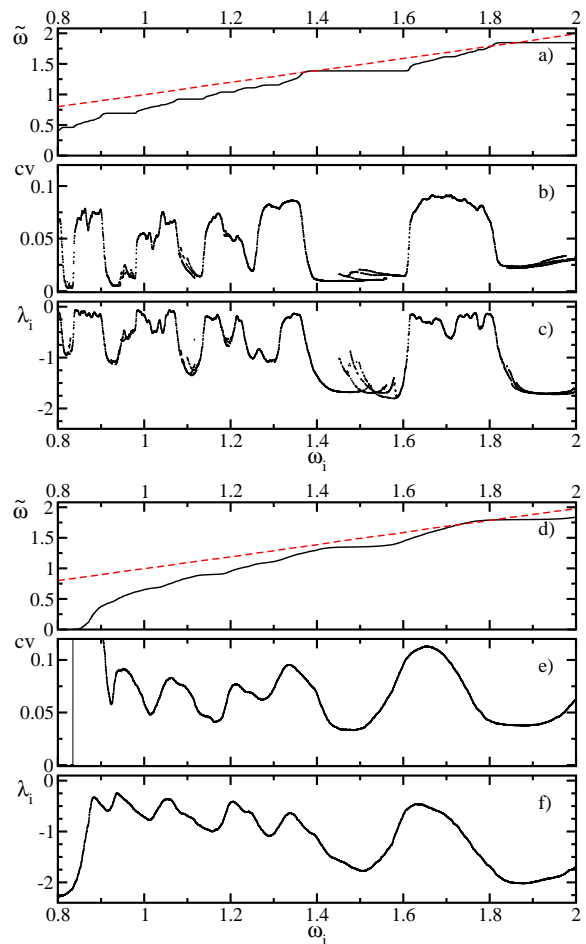


FIG. 8. Effective frequency $\tilde{\omega}$ (panels a and d), CV of $\tilde{\omega}$ (panels b and e) and conditional Lyapunov exponents λ_i (panels c and f) for the different oscillators, for $g = 1$ (panels a-c) and $g = 1.3$ (panels d-f), all for $N = 4000$. The red dashed line in panels a and d show the bare frequency as a reference for the effective frequency shown with solid black lines.

oscillator as a particle moving in a potential with an inclination that depends on its bare frequency and the mean-field E . When two particles with slightly different ω are followed, it may happen that one of them is blocked in a (shallow) minimum which is absent for the other.

One can learn a bit more about the dependence on ω by comparing pairs of consecutive oscillators (consecutive in the space of bare frequencies). This can be done, by monitoring phase slips, i.e. the time instants when the phase difference becomes larger (smaller) than $1/2$ ($-1/2$). Since it is possible that the phase difference may oscillate around $1/2$ ($-1/2$) yielding long sequences of positive and negative slips, we have chosen to record only those events where two or more consecutive positive (negative) slips are observed.

In Fig. 9a we see that for $g = 1$ there exist totally empty bands: they correspond to the previously mentioned synchronization areas. In panel b (which corresponds to $g = 1.3$) both forward and backward slips are simultaneously present.

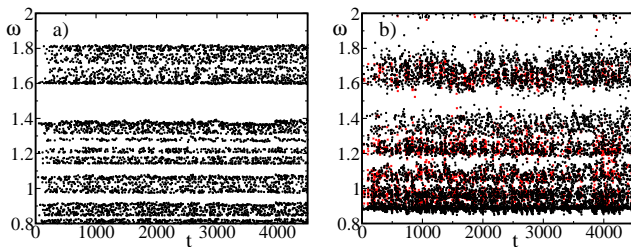


FIG. 9. Phase slips for $g = 1$ (panel a) and $g = 1.3$ (panel b) for $N = 4000$. Black circles correspond to forward slips; red crosses to backward slips, occurring only in panel b.

One can see that the phase slips happen on a much longer time scale than the interspike intervals. Further, the bands with sparse phase slips observed for $g = 1.3$ are reminiscent of the synchronization bands found for $g = 1.0$: there, phase slip events are rare and erratic. The totally empty band at the bottom frequencies for $g = 1.3$ corresponds to the non-firing neurons.

In the thermodynamic limit, the most appropriate way to characterize the collective dynamics is by monitoring the probability distribution $Q(\phi, \omega, t)$ introduced in Sec. III. In Fig. 10 we give an idea of the way it looks like below and above threshold at some randomly chosen time. In panel a) one can recognize a reasonably smooth distribution. In fact, for $g = 0.5$, we are in the asynchronous regime and thereby expect a smooth distribution of the phases ϕ [48]. Such a distribution loses stability above g_c .

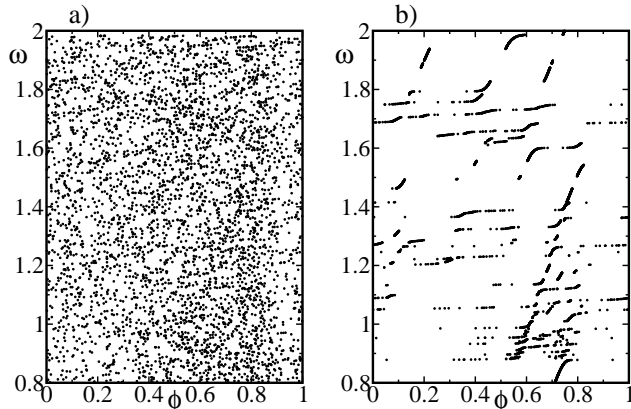


FIG. 10. Snapshots of the probability density $Q(\phi, \omega, t)$ for $g = 0.5$ (panel a) and $g = 1.3$ (panel b) and $N = 4000$.

In fact, for $g = 1.3$ we see a rather different structure (see panel b) characterized by an alternation of highly dense and widely spread regions. It is clear that even the plain integration of the equations (4,5) is a highly nontrivial task, not to speak of the development of approximate analytical schemes.

VI. DISCUSSION AND OPEN PROBLEMS

In this paper we have analysed an ensemble of pulse-coupled oscillators characterized by a distribution of bare frequencies and coupled through a homogeneous mean field. Although the setup is reminiscent of the Kuramoto model, the collective dynamics is much richer and accompanied by a linearly stable microscopic dynamics.

A linear stability analysis of the asynchronous regime allows identifying the transition point beyond which a complex form of synchronization sets in. A numerical analysis of a properly defined Kuramoto order parameter R and of the smoothed activity field Y reveals that they not only fluctuate in time, but their behavior involves a large (possibly infinite) number of degrees of freedom. This indicates that even in “simple” mean-field models, such as the one investigated in this paper, the coarse-grained activity of an ensemble of phase-oscillators cannot be reduced to the evolution of one or a few variables, such as the firing rate and related observables. In principle, nothing prevents a population of phase-oscillators to self-sustain a macroscopic irregular dynamics: the corresponding evolution equation is indeed a nonlinear functional equation (see Eqs. (4,5)), which operates in an infinite-dimensional phase-space. It is, however, unclear under which conditions many degrees of freedom can be simultaneously active. In order to make further progress, it will be necessary to find suitable approximations of the probability density $Q(\phi, \omega, t)$: this task seems to require clever ideas on the way to expand $Q(\phi, \omega, t)$. One question is particularly relevant: whether the dynamics is born high dimensional from the very beginning (such as in models of balanced states [49, 50]) or the complexity increases by undergoing a series of consecutive bifurcations. The numerical analysis in the vicinity of the critical point is affected by too strong finite-size corrections to be able to draw any conclusion.

Another open point is the generality of this scenario. Several preliminary simulations performed with various choices of the PRC reveal that it is quite robust, although the presence of a relatively steep branch seems to be a necessary condition. This is not too serious a limitation, as it naturally appears in systems characterized by a slow-fast dynamics (see the discussion in [51]). It might be, however, worth to assume a different PRC shape to enable deeper analytical studies. We have indeed derived a very general equation for the loss of stability of the asynchronous state: if one could go beyond, including the most relevant nonlinear terms, it should be possible to decide how many degrees of freedom are switched on.

Our numerical studies suggest that the transition disappears when the distribution of frequencies is narrow enough, but this is by no means a proof: understanding whether it is strictly necessary to go beyond the weak-coupling, weak-disorder limit is another point that will be worth exploring.

Another intriguing property of the collective dynamics discussed in this paper is the presence of a spectrum of negative Lyapunov exponents. This means that it is a manifestation of *stable chaos* [29]. Within the context of computational neuroscience, the stability of the microscopic trajectories suggests that this model is a good candidate for performing computa-

tional tasks. It will be worth to explore this opportunity by studying the response of this type of networks to different classes of external stimuli.

ACKNOWLEDGMENT

AP wishes to acknowledge a discussion with M. Wolfrum on the stability of the Kuramoto model.

Appendix A: Stability analysis

The equation (9) for u can be rewritten as

$$\frac{du}{d\phi} = \frac{(g\Gamma'(\phi)E_0 - \mu)u + g[\Gamma'(\phi)Q_0 + \Gamma(\phi)\frac{dQ_0}{d\phi}]z}{\omega - g\Gamma(\phi)E_0}$$

which has the structure

$$\frac{du}{d\phi} = (A - \mu\tau)u + gP(\omega)C(\phi, \omega)z \quad (\text{A1})$$

where

$$A = \frac{g\Gamma'(\phi)E_0}{\omega - g\Gamma(\phi)E_0}, \quad (\text{A2})$$

$$C(\phi, \omega) = \frac{\omega\Gamma'(\phi)}{T(\omega, E_0)(\omega - g\Gamma(\phi)E_0)^3} \quad (\text{A3})$$

while τ is defined in (7). The general solution of Eq. (A1) is

$$u(\phi, \omega) = e^{F(\phi, \omega) - \mu T(\phi, \omega)} [u(0, \omega) + z \int_0^\phi d\psi C(\psi, \omega) e^{-F(\psi, \omega) + \mu T(\psi, \omega)}] \quad (\text{A4})$$

where

$$F(\psi, \omega) = \int_0^\psi d\eta A(\eta) = \log \frac{\omega - g\Gamma(0)E_0}{\omega - g\Gamma(\psi)E_0}, \quad (\text{A5})$$

notice that $F(1) = F(0) = 0$, while $T(\psi, \omega)$ is defined in Eq. (7). One can therefore write the solution $u(\phi, \omega)$ as

$$u(\phi, \omega) = \frac{\omega - g\Gamma(0)E_0}{\omega - g\Gamma(\phi)E_0} e^{-\mu T(\phi, \omega)} [u(0, \omega) + z g P(\omega) \frac{V_\mu(\phi, \omega)}{\omega - g\Gamma(0)E_0}] \quad (\text{A6})$$

where

$$V_\mu(\phi, \omega) = \frac{\omega}{T(1, \omega)} \int_0^\phi d\psi \frac{\Gamma'(\psi) e^{\mu(\psi, \omega)}}{(\omega - g\Gamma(\psi)E_0)^2} \quad (\text{A7})$$

By imposing the periodicity condition $u(1, \omega) = u(0, \omega)$ one obtains

$$u(1, \omega) = g z \frac{P(\omega) V_\mu(1, \omega)(1, \omega)}{(e^{\mu T(1, \omega)} - 1)(\omega - g\Gamma(0)E_0)} \quad (\text{A8})$$

By finally, recalling the definition (10) z , it is possible to rewrite Eq. (A8) as the eigenvalue equation

$$1 + g\Gamma(1) \int Q_0(1, \omega) d\omega = g \int d\omega \frac{P(\omega) V_\mu(1, \omega)}{e^{\mu T(1, \omega)} - 1} \quad (\text{A9})$$

Appendix B: Transformation to the appropriate Kuramoto like phase ϑ

We solve the original system Eq. (1) with the PRC Eq. (2) in terms of the non-homogeneously advancing phase ϕ . At each time point we calculate the Kuramoto order parameter R we convert the phase ϕ into the Kuramoto like phase ϑ according to Eqs. (12) and (13). For simplicity and readability we introduce new constants similar those defining the piecewise linear PRC Eq. (2): $\mathfrak{B}_{01} = \frac{\tilde{\omega}}{N} E_0 B_{01}$, $\mathfrak{B}_{02} = \frac{\tilde{\omega}}{N} E_0 B_{02}$, $\mathfrak{B}_{03} = \frac{\tilde{\omega}}{N} E_0 B_{03}$, $\mathfrak{b}_1 = \frac{\tilde{\omega}}{N} E_0 b_1$, and $\mathfrak{b}_2 = \frac{\tilde{\omega}}{N} E_0 b_2$. Hence the Kuramoto like phase is

$$\vartheta(\phi(t)) = \begin{cases} \frac{\tilde{\omega}}{\mathfrak{b}_1} \ln \frac{\omega - \mathfrak{B}_{01}}{\omega - \mathfrak{B}_{01} - \mathfrak{b}_1 \phi(t)} & \text{if } 0 \leq \phi < \phi_l \\ \vartheta_l - \frac{\tilde{\omega}}{\mathfrak{b}_2} \ln \frac{\omega - \mathfrak{B}_{02} + \mathfrak{b}_2 \phi(t)}{\omega - \mathfrak{B}_{02} + \mathfrak{b}_2 \phi_r} & \text{if } \phi_l \leq \phi \leq \phi_r \\ \vartheta_r + \frac{\tilde{\omega}}{\mathfrak{b}_1} \ln \frac{\omega - \mathfrak{B}_{03} - \mathfrak{b}_1 \phi_r}{\omega - \mathfrak{B}_{03} - \mathfrak{b}_1 \phi(t)} & \text{if } \phi_r < \phi < 1, \end{cases}$$

with the field E_0 as stated in Eq. (8) and the effective frequency defined as the inverse interspike interval, i.e. $\tilde{\omega} = 1/T(1, \omega, E_0)$ (Eq. (7)). The interspike interval can be expressed explicitly for the give PRC:

$$T(1, \omega, E_0) = \frac{1}{\mathfrak{b}_1} \ln \frac{\omega - \mathfrak{B}_{01}}{\omega - \mathfrak{B}_{01} - \mathfrak{b}_1 \phi_l} - \frac{1}{\mathfrak{b}_2} \ln \frac{\omega - \mathfrak{B}_{02} + \mathfrak{b}_2 \phi_l}{\omega - \mathfrak{B}_{02} + \mathfrak{b}_2 \phi_r} + \frac{1}{\mathfrak{b}_1} \ln \frac{\omega - \mathfrak{B}_{03} - \mathfrak{b}_1 \phi_r}{\omega - \mathfrak{B}_{03} - \mathfrak{b}_1}$$

As shown in Fig. 1, the transitions ϑ_l and ϑ_r in the effective PRC $\tilde{\Gamma}$ depend on the bare frequency ω according to:

$$\vartheta_l = \frac{\tilde{\omega}}{\mathfrak{b}_1} \ln \frac{\omega - \mathfrak{B}_{01}}{\omega - \mathfrak{B}_{01} - \mathfrak{b}_1 \phi_l}$$

$$\vartheta_r = \vartheta_l - \frac{\tilde{\omega}}{\mathfrak{b}_2} \ln \frac{\omega - \mathfrak{B}_{02} + \mathfrak{b}_2 \phi_l}{\omega - \mathfrak{B}_{02} + \mathfrak{b}_2 \phi_r}.$$

- [2] C. van Vreeswijk, *Phys. Rev. E* **54**, 5522 (1996).
- [3] A. Politi and M. Rosenblum, *Phys. Rev. E* **91**, 042916 (2015).
- [4] D. Hansel, G. Mato, and C. Meunier, *Neural Comput.* **7**, 307 (1995).
- [5] H. Daido, *Prog. Theor. Phys.* **88**, 1213 (1992); **89**, 929 (1993); *Physica D* **91**, 24 (1996).
- [6] H. Wilson and J. Cowan, *Biophys. J.* **12**, 1 (1972).
- [7] S. Coombes, *Biological Cybernetics* **93**, 91 (2005).
- [8] B. G.B. Ermentrout and D. Terman, *Mathematical foundations of neuroscience*, Vol. 35 (Springer, New York, 2010).
- [9] T. Luke, E. Barreto, and P. So, *Neural computation* **25**, 3207 (2013).
- [10] P. So, T. B. Luke, and E. Barreto, *Physica D: Nonlinear Phenomena* **267**, 16 (2014), *evolving Dynamical Networks*.
- [11] C. R. Laing, *Phys. Rev. E* **90**, 010901 (2014).
- [12] E. Montbrió, D. Pazó, and A. Roxin, *Phys. Rev. X* **5**, 021028 (2015).
- [13] E. Ott and T. M. Antonsen, *Chaos* **18**, 037113 (2008).
- [14] S. Watanabe and S. H. Strogatz, *Physica D: Nonlinear Phenomena* **74**, 197 (1994).
- [15] A. Arieli, D. Shoham, R. Hildesheim, and A. Grinvald, *Journal of Neurophysiology* **73**, 2072 (1995).
- [16] M. Tsodyks, T. Kenet, A. Grinvald, and A. Arieli, *Science* **286**, 1943 (1999).
- [17] A. Destexhe, *Current Opinion in Neurobiology* **21**, 717 (2011).
- [18] M. N. Shadlen and W. T. Newsome, *The Journal of Neuroscience* **18**, 3870 (1998).
- [19] D. A. Butts, C. Weng, J. Jin, C.-I. Yeh, N. A. Lesica, J.-M. Alonso, and G. B. Stanley, *Nature* **449**, 92 (2007).
- [20] C. van Vreeswijk and H. Sompolinsky, *Science* **274**, 1724 (1996).
- [21] C. van Vreeswijk and H. Sompolinsky, *Neural Computation* **10**, 1321 (1998).
- [22] T. Shibata, T. Chawanya, and K. Kaneko, *Phys. Rev. Lett.* **82**, 4424 (1999).
- [23] K. A. Takeuchi and H. Chaté, *J. Phys. A* **46**, 254007 (2013).
- [24] S. Luccioli and A. Politi, *Phys. Rev. Lett.* **105**, 158104 (2010).
- [25] Y. Kuramoto, *Chemical Oscillations, Waves and Turbulence* (Springer, Berlin, 1984).
- [26] J. A. Acebron, L. L. Bonilla, C. J. P. Vicente, F. Ritort, and R. Spigler, *Rev. Mod. Phys.* **77**, 137 (2005).
- [27] M. Komarov and A. Pikovsky, *Physica D: Nonlinear Phenomena* **289**, 18 (2014).
- [28] P. Ashwin and O. Burylko, *Chaos* **25**, 013106 (2015).
- [29] A. Politi and A. Torcini, in *Nonlinear dynamics and chaos: advances and perspectives*, Underst. Complex Syst. (Springer, Berlin, 2010) pp. 103–129.
- [30] R. Zillmer, R. Livi, A. Politi, and A. Torcini, *Phys. Rev. E* **74**, 036203 (2006).
- [31] S. Jahnke, R.-M. Memmesheimer, and M. Timme, *Phys. Rev. Lett.* **100**, 048102 (2008).
- [32] R. Zillmer, N. Brunel, and D. Hansel, *Phys. Rev. E* **79**, 031909 (2009).
- [33] M. Monteforte and F. Wolf, *Phys. Rev. Lett.* **105**, 268104 (2010).
- [34] M. Monteforte and F. Wolf, *Phys. Rev. X* **2**, 041007 (2012).
- [35] L. F. Abbott and C. van Vreeswijk, *Phys. Rev. E* **48**, 1483 (1993).
- [36] S. Strogatz and R. Mirollo, *Journal of Statistical Physics* **63**, 613 (1991).
- [37] S. H. Strogatz, R. E. Mirollo, and P. C. Matthews, *Phys. Rev. Lett.* **68**, 2730 (1992).
- [38] H. Chiba, *Ergodic Theory Dynam. Systems* **35**, 762 (2015).
- [39] B. Fernandez, D. Gérard-Varet, and G. Giacomini, “Landau damping in the kuramoto model,” (2014), arXiv:1410.6006.
- [40] H. Dietert, “Stability and bifurcation for the kuramoto model,” (2015), arXiv:1411.3752v2.
- [41] M. K. S. Yeung and S. H. Strogatz, *Phys. Rev. Lett.* **82**, 648 (1999).
- [42] M. Y. Choi, H. J. Kim, D. Kim, and H. Hong, *Phys. Rev. E* **61**, 371 (2000).
- [43] R. Badii and A. Politi, *Journal of Statistical Physics* **40**, 725 (1985).
- [44] R. Hegger, H. Kantz, and T. Schreiber, *Chaos* **9**, 413 (1999).
- [45] S. Olmi, R. Livi, A. Politi, and A. Torcini, *Phys. Rev. E* **81**, 046119 (2010).
- [46] As stated previously, they are not truly phase-locked since the phase difference fluctuates.
- [47] E. Ullner, A. Zaikin, E. I. Volkov, and J. García-Ojalvo, *Phys. Rev. Lett.* **99**, 148103 (2007); A. Koseska, E. Volkov, and J. Kurths, *Physics Reports* **531**, 173 (2013).
- [48] A perfect uniformity would be observed if the effective phases ϑ were to be used - see the appendix B for their definition.
- [49] H. Sompolinsky, A. Crisanti, and H.-J. Sommers, *Phys. Rev. Lett.* **61**, 259 (1988).
- [50] G. Curato and A. Politi, *Phys. Rev. E* **88**, 042908 (2013).
- [51] P. Langfield, B. Krauskopf, and H. M. Osinga, *SIAM J. Appl. Dyn. Syst.* **14**, 1418 (2015).